Journal of Magnetic Resonance **138,** 210–219 (1999)
Article ID jmre.1999.1738, available online at http://www.idealibrary.com on IDEAL®

Linewidth Analysis of Spin Labels in Liquids

II. Experimental

B. H. Robinson, C. Mailer, and A. W. Reese

Department of Chemistry, University of Washington, Seattle, Washington 98195

Received July 28, 1998; revised February 12, 1999

This work demonstrates that homogeneous linewidths can be extracted from continuous wave electron paramagnetic resonance spectra and that they quantitatively agree with the predictions of existing relaxation theory. We suggest that relaxation theory can be used to predict experimental lineshapes provided that the simulations properly include sources of broadening. We have found that the rotational correlation times for spin labels in different percentages of glycerol/water mixtures are best modeled by a power law treatment for the viscosity, similar to that for translational diffusion. The translational diffusion coefficients themselves also have a power law dependence on the viscosity for glycerol/water mixtures. The linewidths were linearly dependent upon both the oxygen and the spin label concentration. The hyperfine splittings of all nuclei were observed to decrease linearly with increasing spin label concentration, completely at odds with existing theory which predicts a quadratic dependence upon concentration. The linear dependence was independent of hyperfine splitting until the magnitude of the hyperfine splitting was less than the homogeneous linewidth.

Key Words: **linewidth; EPR spin labels; simulations exchange.**

INTRODUCTION

Continuous wave electron paramagnetic resonance (CW-EPR) using nitroxide spin labels is capable of measuring the rotational correlation times of molecules in solution over many orders of magnitude. Oftentimes, when simulating EPR spectra to obtain the motional information, the linewidths are left as adjustable parameters. The basic theory of linewidths in solution was worked out by Freed and co-workers (*1*) based on the Redfield theory (*2*). In Freed's seminal papers, the theory for the linewidths always allowed for an extra adjustment factor, X. We have revisited the need for such an extra mechanism. Experimentally the observed linewidths are always broader than Freed theory predicts—the extra broadening results from a combination of unresolved hyperfine coupling, concentration of spin label and other paramagnetic molecules, and instrumental effects. With an optimized lineshape simulation procedure, described in Paper I, the companion paper to this one (*3*), we were able to fit experimental EPR spectra including all spectrometer and inhomogeneous broadening effects directly in the simulations. From these fitted spectra we extracted homogeneous linewidths which agreed with those calculated by the theory developed by Freed. Preliminary results have been presented elsewhere (*4*).

To guarantee that the linewidth model does indeed fit over a wide range of rotational correlation times we adopted the protocol used by others (*1, 5*): The spin labels were placed in a variety of mixtures of water and glycerol. This presented an additional challenge as it has been observed that in high-percentage glycerol solutions the rotational dynamics do not obey the simple Stokes–Einstein equation (*6*). Moreover, it has been observed that additional broadening mechanisms due to the oxygen and nitroxide do not appear to obey the Stokes–Einstein law either (*5, 7*). There seems to be no way to systematically move from pure water, in which Stokes–Einstein is obeyed, to high-percentage glycerol solutions.

What would the linewidths of nitroxides be if there were no broadening mechanisms acting other than rotational motion on a single nitroxide spin label? The apparent linewidth as a function of nuclear quantum number, m, is (*1*)

$$R_{2eo}(m) = A' + A(m) + B(m) \cdot m + C(m) \cdot m^2 + X(m), \quad [1]$$

where A, B, and C may be weakly m-dependent quantities derived from both the anisotropic part of the CSA (chemical shift anisotropy) and the END (electron-nuclear dipolar) coupling terms calculated from the g and A values and the rotational correlation time. A' is the contribution to the linewidth from the g-value-dependent spin rotational mechanism, which has an approximate inverse dependence upon the rotational correlation time. X is any linewidth contributions from other broadening processes. The Freed work concentrated mainly on explaining the values of A, B, and C in terms of particular detailed motional models applying the appropriate spectral density functions to the CSA and END mechanisms. Their theory has been programmed in MATLAB and representative results are plotted in Fig. 1 (*8*); an important finding is the

1090-7807/99 $30.00

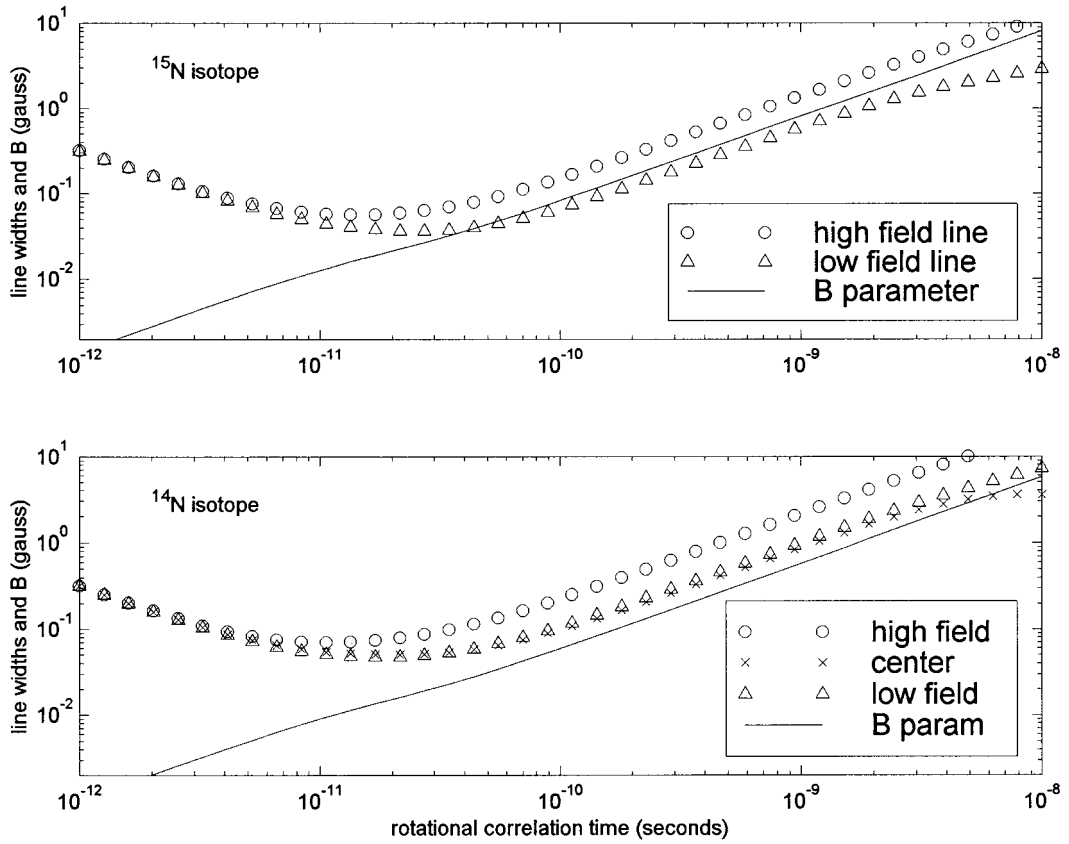

FIG. 1. (Top) Fundamental EPR linewidths, R_{2eo}, for an ^{15}N ($m = +\frac{1}{2}$ and $-\frac{1}{2}$) spin system versus rotational correlation time are plotted. The *B* parameter—numerically equal to the difference of the $m = -\frac{1}{2}$ and $m = +\frac{1}{2}$ linewidths is also shown. The same *g* values and motional model as for the ^{14}N calculation (bottom) were used but the *A* values were increased to 8, and 7, and 47 G. (Bottom) Fundamental EPR linewidths, R_{2eo} for an ^{14}N ($m = 0, +1$, and -1) spin system versus rotational correlation times are plotted. The *B* parameter—numerically equal to half the difference of the $m = -1$ and $m = +1$ linewidths is also shown. The *g* values were 2.008, 2.006, and 2.0023, the *A* values were 7, 6, and 32 G, and the rotational motion was assumed to be isotropic. The microwave frequency was 9.4 GHz, at X band.

linearity between the rotational correlation time and the *B* parameter as shown.

Effects of glycerol. CW EPR spectra are sensitive functions of the rotational correlation times. To change the rotational correlation time over four orders of magnitude, as was done in these studies, it was necessary to place the small spin labels in solutions of various percentages of glycerol. Simple Stokes–Einstein (SE) theory says that the rotational correlation time $\tau_\theta = \frac{4}{3}(\pi r_o^3 \eta/kT)$, where r_o is the hydrodynamic radius of the molecule, η is the solution viscosity, T the absolute temperature, and k the Boltzmann constant. Hwang *et al.* (*1*) reported that the perdeuterated spin label TEMPONE (2,2,6,6-tetramethyl-4-piperidone *N*-oxide) moved much faster in pure glycerol than predicted from the bulk viscosity. The effective rotational radius, r_e, was obtained from the rotational SE relation $\tau_\theta = \frac{4}{3}(\pi r_e^3 \eta/kT) = \kappa \frac{4}{3}(\pi r^3 \eta/kT)$ where κ is a "slip factor" ($0 \leq \kappa \leq 1$) suggested by Kivelson (*6*) and was found to be about 0.13—meaning that the spin label moved some 7.5 times faster than expected in 100% glycerol than the bulk viscosity would predict. Subczynski and Hyde (*5*) showed that the slopes of plots of correlation time as a function of η/T for a fixed percentage of glycerol were a weak function of the glycerol percentage; they appeared to obey a reduced power law dependence on η, i.e., the correlation time was proportional to $(\eta/T)^{\text{power}}$, with power < 1. These workers also found that while the translational diffusion of O_2 in water obeyed SE, it did not obey SE in a variety of oils. O_2 diffusion also obeys a power law dependence on (η/T) with power < 1. Subczynski and Hyde suggested that the effects of solvents are best seen by assuming that the translational diffusion time, τ_{trans}, is proportional to the viscosity raised to a power, p: $\tau_{\text{trans}} = A\eta^p$. This is based on the work of Evans *et al.* (*9*), who carried out extensive studies on the variation of solute translational diffusion coefficients for solutes of different radii in a number of solvents over a wide range of viscosities. The Stokes–Einstein expression for the translational diffusion coefficient D_{trans} is

$$D_{\text{trans}} = kT/6\pi\eta r. \qquad [2]$$

This SE equation failed when the solute molecules were comparable to (or less than) the size of the solvent molecules. Evans *et al.* (*9*) developed empirical equations for the relationship between the diffusion coefficient, the viscosity, and the radius of the solute:

$$D_{\text{trans}} = AT/\eta^p, \qquad [3]$$

where A is an arbitrary constant. Evans also suggested the following empirical relationship relating the viscosity exponent p to the molecular radius, r in Å:

$$p = 1.166 - (1.296/r). \qquad [4]$$

We have chosen to extend, and slightly modify, this approach so that both translational and rotational correlation times are similar functions of the glycerol percentage. For the translational diffusion coefficient we can write

$$D_{\text{trans}} = D^{\text{o}}_{\text{trans}}\left(\frac{\eta_{\text{o}}}{\eta}\right)^p. \qquad [5]$$

Here, D^{o} is the diffusion coefficient for the solute in pure water at a specified temperature, while η and η_{o} are, respectively, the viscosity of the solution at the same temperature with and without glycerol. For the rotational correlation time, we assume an equation of the form

$$\tau_\theta = \frac{4}{3}\frac{\pi r^3_{\text{o}}\eta_{\text{o}}}{kT}\left(\frac{\eta}{\eta_{\text{o}}}\right)^p, \qquad [6]$$

where $\eta_{\text{o}} = \eta\ (\phi = 0)$ and the power p of the viscosity is a function of the volume fraction of glycerol, ϕ. This form of the correlation time equation is superior to one containing $(\eta/T)^p$ as it is dimensionally correct, but still allows for nonunity p and permits the correlation time to follow SE theory when the solvent is pure water. The volume fraction of glycerol, ϕ is given by the empirical relation

$$p(\phi) = \frac{p_1}{p_1 + (1 - p_1)\phi^{1/8}}, \qquad [7]$$

where $p(\varphi = 0) = 1$ and $p(\varphi = 1) = p_1$. The $\frac{1}{8}$ power dependence of p on ϕ was chosen so that the function would move very quickly to its limiting value, p_1, for $\phi > 0.2$, from its value of unity in pure water (where $\phi = 0$), as suggested by the work of Evans *et al.* (*9*) and Jordan *et al.* (*10*). The weight fraction of glycerol, f, is converted to the volume fraction ϕ using the expression $\phi = f/(s - (s - 1)f)$; s is the specific gravity of glycerol. Equation [6] can then be written, in analogy with Eq. [5], as

$$\tau_\theta = \tau_{\text{o}}\left(\frac{\eta}{\eta_{\text{o}}}\right)^p, \qquad [8]$$

where τ_{o} is the rotational correlation time of the nitroxide in water (0% glycerol) and η_{o} is the viscosity of water at the same temperature. We further assume that τ_{o} and $D^{\text{o}}_{\text{trans}}$ obey the SE relation in pure water. We do not assume that the p_1 governing the rotational diffusion is the same as that for translational diffusion.

Concentration of paramagnetic molecules. The exchange of spin states produced by molecular collision is a stochastic process which leads to an increased linewidth. The standard model used to fit the concentration dependence of the linewidth data is

$$R_{2\text{e}} = R_{2\text{eo}} + R_{2\text{e}}(\text{label}) + R_{2\text{e}}(\text{oxygen}), \qquad [9]$$

where $R_{2\text{eo}}$ is the linewidth from Eq. [1] (*1*), shown in Fig. 1, and $R_{2\text{e}}$(label) and $R_{2\text{e}}$(oxygen) are the linewidth broadening produced by label–label and label–oxygen collisions, respectively.

The effective relaxivity is (*11*) $\text{SF} \cdot K_{\text{ex}}$ and

$$R_{2\text{e}}(X) = \text{SF}(X) \cdot [X] \cdot K_{\text{ex}}, \qquad [10]$$

Where $[X]$ is the concentration of the broadening species—label or oxygen. K_{ex} is the exchange constant for the process and depends upon the exchange integral overlap and lifetime of the collision (*12, 13*). SF, the statistical factor, governs what fraction of collisions produce an observable change in magnetization. The SF is only needed for the collision of identical species, and so SF = 1 when considering the relaxation due to $[O_2]$. For example the SF for $^{15}ND_{13}$–$^{15}ND_{13}$ collisions is $\frac{1}{2}$ because only $|+\frac{1}{2}\rangle \Leftrightarrow |-\frac{1}{2}\rangle$ collisions are effective in broadening, whereas collisions between $|+\frac{1}{2}\rangle \Leftrightarrow |+\frac{1}{2}\rangle$ and $|-\frac{1}{2}\rangle \Leftrightarrow |-\frac{1}{2}\rangle$ are not. Table 1 shows the statistical factors for several cases. $^{15}ND_{12}H_1$ (**II** in Fig. 2) means that the ^{15}N spin label is fully deuterated except for a proton at the axial position of the ring (*14*).

EXPERIMENTAL

Spin labels. Figure 2 shows the structures of the spin labels employed in this work. Most of the experiments were done with spin labels (**I**): ^{15}N fully deuterated CTPO, (2,2,5,5-tetramethyl-3-pyrrolin-d_{13}, 1-^{15}N-1-oxyl-3-carboxamide) (CDN Isotopes, Canada) and (**II**): ^{15}N-deuterated CTPO (gift of Dr. Howard Halpern), in which only the single-ring hydrogen remains protonated. The line splitting in the EPR spectrum due to the single-ring proton can be seen clearly. The ^{14}N CTPO

TABLE 1
Statistical Factors and Relaxivities for Nitroxide Species

Isotope	$^{15}ND_{13}$ (**I**)	$^{15}ND_{12}H_1$ (**II**)	$^{14}NH_{13}$ (**III**)	$^{14}ND_{12}H_1$ (**IV**)	$^{14}ND_{13}$ (**V**)
SF nitrogen only	1/2	1/2	2/3	2/3	2/3
Relative SF[a]	100	100	133	133	133
SF N + extra species	1/2[b]	3/4	5/6	5/6	2/3[b]
Relative SF	100	150	166	166	133
Experimental relaxivity mG/mM[f]	100[d]	120[d]	128[d]	144[e]	130[c]
Relative relaxivity[g]	1	1.2	0.96	1.1	0.98

[a] The relative statistical factor due to [NO] is defined as (ratio of the statistical factor for the appropriate isotope to that of the $^{15}ND_{13}$ spin label) × 100.
[b] Deuteron hfs is too small to produce a change in the SF from nitrogen only.
[c] A. Smirnov, personal communication.
[d] This work.
[e] Reference (*14*).
[f] The experimental relaxivity is determined for each of these spin labels in water at 20°C. The measured relaxivity was found to be independent of $[O_2]$.
[g] Relative relaxivity is the experimental relaxivity (row 5)/(200 ∗ SF), where the SF is for the nitrogen-only case, row 1.

spin labels 2,2,5,5-tetramethyl-3-pyrrolin-1-^{14}N-1-oxyl-3-carboxamide, (**III**), and the deuterated version (**V**) have been used for EPR oximetry (*15*). Halpern *et al.* (*14*) used monoprotonated ^{14}N CTPO (**IV**) in their oxygen concentration studies. Solutions were made up of various spin label concentrations of spin label in water and in 15, 40, 50, 70, and 90% glycerol (w/w). The TEMPOL spin label also used (**VI**): 4-hydroxy-2,2,6,6-tetramethyl piperidine-d_{16} 1-^{15}N-1-oxyl was made up in water and in 20, 60, 70, 80, 90, and 95% glycerol (w/w).

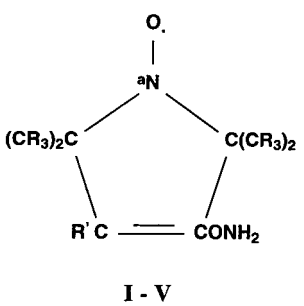

	R	R'	a
I	D	D	15
II	D	H	15
III	H	H	14
IV	D	H	14
V	D	D	14

I - V

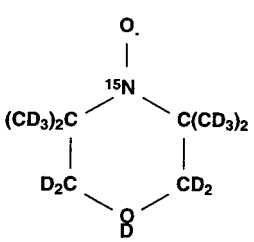

VI

FIG. 2. Spin labels used: (**I**) $^{15}ND_{13}$ fully deuterated CTPO, (2,2,5,5-tetramethyl-3-pyrrolin-d_{13}, 1-^{15}N-1-oxyl-3-carboxamide) (CDN Isotopes, Canada); (**II**) $^{15}ND_{12}H_1$-deuterated CTPO, fully deuterated except for the protonated single-ring hydrogen (gift of Dr. Howard Halpern). The ^{14}N spin labels are (**III**) CTPO,2,2,5,5-tetramethyl-3-pyrrolin-1-^{14}-1-oxyl-3-carboxamide, the monoprotonated version (**IV**), and the deuterated version (**V**). The TEMPOL spin label was also used (**VI**): 4-hydroxy-2,2,6,6-tetramethyl piperidine-d_{16} 1-^{15}N-1-oxyl.

EPR spectrometer. The samples were studied using a Bruker EMX (Bruker, Inc, Billerica, MA) spectrometer with a standard TE_{102} cavity. For accurate measurements of spin lattice relaxation a pulse spectrometer containing a loop gap resonator (LGR from Medical Advances, Milwaukee, WI) was used (*16*). Typical CW EPR settings were 32 G sweep range, 10 kHz modulation frequency, 0.050 G peak-to-peak modulation amplitude, 1024 data points, microwave powers of 0 or −10 dBm giving observer RF field amplitude h_1 of 0.0420 or 0.015 G, respectively. Data were collected at room temperature and at least three spectra were collected for each set of conditions. The experimental uncertainties were calculated based on replicate runs and are reported numerically in the text or as error bars in the figures.

Experimental protocol. A range of spin label concentrations were made up in the appropriate liquid, e.g., water, 15% glycerol–water, etc. Samples 25 mm long were drawn up into 0.8-mm OD × 0.6-mm ID quartz tubes and sealed at each end. The tubes were placed in a slotted plastic holder designed to hold samples for air removal experiments. Spectra were run with air flowing through the cavity dewar at a known temperature and spectra were simulated with the CW linewidth fitting program (see Paper I (*3*)). Concentrations were checked against samples of 0.5 and 1 mM monoprotonated ^{15}N *d*CTPO (**II**). The TEMPOL experiments were done with 1 mM concentration of label. For deoxygenation experiments 25-mm-long samples were injected into thin-walled 22 AWG diameter Teflon tubing (*17*). Such tubing in the slotted plastic holder allowed air/nitrogen exchange between sample and gas flowing (*15*). Nitrogen was passed through the cavity and spectra were run until the linewidths had attained their constant values. Usually this took about 30–40 min due to the wall thickness of the tubing (*18*). Deoxygenation changed concentrations by less than 2%.

Fitting data. The data were fit using the optimizing protocol developed in Paper I (*3*), which took into account the additional sources of linewidth broadening caused by the instrumentation of the EPR experiment:

(i) absorption/dispersion microwave phase rotation;
(ii) observer RF field amplitude h_1;
(iii) Zeeman modulation frequency, modulation amplitude, and phase;
(iv) inhomogeneous broadening due to unresolved hyperfine splitting from neighboring nuclei, which is a source of linewidth broadening intrinsic to the molecules in solution.

RESULTS

Broadening vs spin label concentration in water. Row 5 of Table 1 shows the experimentally measured relaxivities arising from bimolecular spin label nitroxide collisions in water. The theoretical statistical factors for relaxation due to nitrogen only are in row 1 and for nitrogen plus the protons in row 3. We assumed that deuterons did not contribute to the statistical factors in row 3. Comparison of row 2 with row 5 shows that the relaxivity follows the statistical factors for nitrogen only. We find that the relative relaxivity (row 6) is reasonably constant for all five isotopically different samples: The labels protonated at the axial position show an extra contribution to the broadening. This is because the proton hfs of 0.5 G is large enough to produce an extra splitting that increases the statistical factors as indicated in row 3 of Table 1. Experimentally, the axial proton splitting does increase slightly the relaxivity but not as much as predicted (row 3), perhaps because the lines are not clearly resolved. None of the 12 methyl protons or deuterons appear to contribute to homogeneous broadening through the relaxivity term.

Broadening vs oxygen concentration in water. There have been many measurements of the effectiveness of oxygen in broadening EPR lines (*19*). Recent results are tabulated in Table 2; the relaxivity is the broadening expressed in milligauss per millimolar oxygen (mG/mM). Table 2 shows the broadening of the true Lorentzian linewidth, and not the peak-to-peak derivative linewidth often quoted (which is $2/\sqrt{3}$ times greater). Table 2 demonstrates that oxygen appears to be a very effective relaxer of spin labels, some four to five times better than spin labels. However the fundamental mechanisms are not as different as they might seem as we now demonstrate.

Following Abragam (*20*), the total relaxivity is $R_{2e}(X)/[X] = \mathrm{SF}(X) \cdot S(S+1) \cdot K_o(X)$, where X stands for O_2, ^{15}N, or ^{14}N. $K_o(X)$ is the fundamental relaxivity of either species, which includes collision radius and relative diffusion (*11*). S is the total electron spin of the species (*20*). When oxygen collides with a spin label the $\mathrm{SF}(O_2)$ is unity, independent of the labels' spin state, because the relaxation time of the oxygen is very much less than the lifetime of the collision (*5*, *13*). The electronic spin of oxygen is unity, twice that of the spin label.

TABLE 2
Relaxivity of Oxygen with Spin Labels in Water for the Temperatures Shown

Spin label/Isotope	Temperature (°C)	O_2 relaxivity (mG/mM)	O_2 relaxivity (mG/mM[b])	Reference
$^{14}NH_{16}$	4–60	258–284[a]	—	(*5*)
$^{14}NH_{13}$	37	470	432	(*24*)
$^{14}NH_{13}$	20	441	441	This work
$^{14}ND_{12}H_1$	room	501	501	(*25*)
$^{14}ND_{12}H_1$	27	476	463	(*26*)
$^{14}NH_{13}$	22	468	465	(*27*)
$^{15}ND_{13}$	37	463	426	(*28*)
$^{15}ND_{13}$	20	420 ± 20	420 ± 20	This work

[a] Linewidths not corrected for inhomogeneous broadening.
[b] Relaxivities corrected to 20°C based on oxygen solubility and viscosity of water (*29*).

We can therefore write the ratio of relaxivities for an $^{15}ND_{13}$ label colliding with oxygen:

$$\frac{420}{100} = \frac{\mathrm{SF}(O_2) \cdot S(S+1) \cdot K_o(O_2)}{\mathrm{SF}(^{15}N) \cdot S(S+1) \cdot K_o(^{15}N)} = \frac{1 \cdot 2 \cdot K_o(O_2)}{1/2 \cdot 3/4 \cdot K_o(^{15}N)}. \quad [11]$$

Rearranging and solving we obtain $K_o(O_2)/K_o(^{15}N) = 0.79$. For ^{14}N the ratio of relaxivities is approximately 441/128, and the $\mathrm{SF}(^{14}N) = \frac{2}{3}$ leading to $K_o(O_2)/K_o(^{14}N) = 0.86$. Hence oxygen and spin labels have nearly identical relaxivities once statistical and spin factors are taken into account. $K_o(X)$ is proportional to: (i) the relative translational diffusion, which is about 25% larger for O_2 than spin labels; (ii) the collision probability, and (iii) the collision radius, the ratios of which are on the order of unity. As a result the spin exchange mechanisms leading to relaxation for these two species appear to be very similar.

Linewidth dependence upon spin label and oxygen concentration at different viscosities. We can investigate the kinetics of the collision interactions by measuring the linewidths versus the spin label concentration for several solvent viscosities. From Eq. [1] for ^{15}N spin labels we define $\bar{R}_{2eo}$ as $\bar{R}_{2eo} = (R_{2eo}(\frac{1}{2}) + R_{2eo}(-\frac{1}{2}))/2 = A' + A + \frac{1}{4}C$, which enables calculations to be done independent of m. To analyze our data we adopted the Evans model given in Eqs. [3] and [8], which begins with the translational diffusion coefficient obeying Stokes–Einstein in water. In the presence of glycerol, the dependence of the diffusion coefficient should have a reduced dependence on the viscosity as suggested in Eq. [8]. Following Hyde and Subczynski (*19*) we fit our data to a model of the form

$$\bar{R}_{2e}^{\mathrm{calc}} = \bar{R}_{2eo} + 2 \cdot C_{NO}[NO]D_{NO} + C_{O_2}[O_2]\{D_{O_2} + D_{NO}\}, \quad [12]$$

where D_{NO} and D_{O_2} are the translational diffusion coefficients of the spin label and the O_2, respectively. The dependence upon viscosity, temperature, and percentage of glycerol are given by Eq. [5]. The constants C_{NO} and C_{O_2} should be proportional to the interaction distance of the molecules (*19*). Direct substitution of the definitions of the diffusion coefficients into Eq. [12] gives the predicted dependence of the relaxation rate on the viscosity and temperature:

$$\bar{R}_{2e}^{calc} = \bar{R}_{2eo} + 2 \cdot C'_{NO}[NO] \frac{T}{T_o} \left(\frac{\eta_o}{\eta}\right)^a + C'_{O_2}[O_2] \frac{T}{T_o} \times \left\{ \left(\frac{\eta_o}{\eta}\right)^a + \left(\frac{r_{NO}}{r_{O_2}}\right)\left(\frac{\eta_o}{\eta}\right)^b \right\}, \quad [13]$$

where $2C'_{NO}$ and $C'_{O_2}(1 + (r_{NO}/r_{O_2}))$ are the relaxivities in water at $T = T_o$. The exponents a and b are determined from experiment and are functions of the percentage of glycerol, ϕ, following Eq. [7]:

$$a = a(\phi) = \frac{a_1}{a_1 + (1 - a_1)\phi^{1/8}} \quad \text{and}$$

$$b = b(\phi) = \frac{b_1}{b_1 + (1 - b_1)\phi^{1/8}}.$$

Measurement of rotational correlation time. For the ^{15}N label the B parameter is the difference of the two linewidths and, for the ^{14}N, B is half of the difference of the high- and low-field linewidths. τ_θ is calculated from B using the Goldman equations (*1*). Figure 1 shows that the B parameter is a good measure of the rotational correlation time (τ_θ), the two being virtually proportional, with a slope of about 1 ps/mG over the motional range from 10^{-11} to 10^{-9} seconds for both ^{14}N and ^{15}N isotopes. Note that the proportionality is maintained on the fast side of the linewidth minimum, down to very small B values. The linewidths themselves are also functions of τ_θ and therefore the values of τ_θ estimated from the linewidths must agree with those predicted by the B parameter.

Experimental data and the predictions of the modified Stokes–Einstein Eq. [6] are shown in Fig. 3A, which is a log–log plot of τ_θ for TEMPOL, determined via the experimental B parameter, as a function of (η/T) for various glycerol/water mixtures at two different temperatures. The deviation from a slope of unity, and hence disagreement with classical SE behavior, is clearly visible. In contrast to the SE model, the Evans' model of Eq. [6] with a single value of $p_1 = 0.7$ fits both sets of data reasonably well. We originally tried to fit these data to the slip factor model (*1, 21*) but found that such a model could not give a fit that was consistent with both the 19°C data and the −6°C data.

Figure 3B shows the analogous data for the deuterated ^{15}N CTPO spin label (**I**) where we plot τ_θ/τ_o against (η/T). These axes were chosen to magnify small differences in the viscosity power law: the SE relation is a horizontal line and the predictions of the Evans model of Eq. [6] appear as negative slopes. We note that if we had simply pooled all of the data, regardless

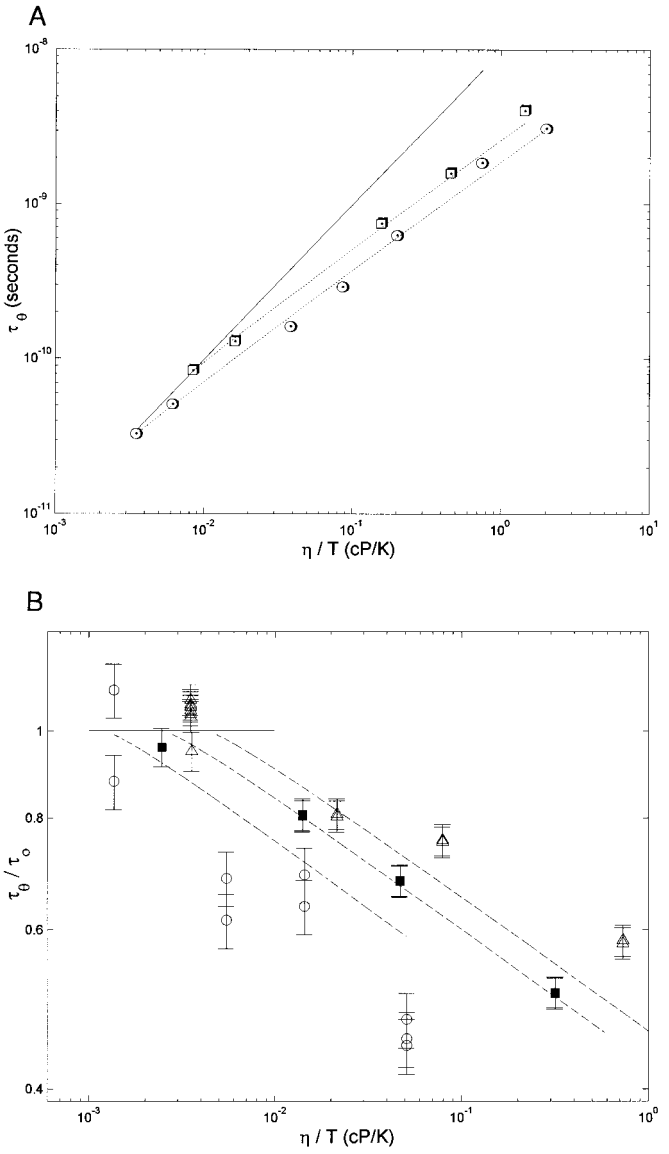

FIG. 3. (A) Rotational correlation times, τ_θ, in seconds, versus η/T, in units of cP/°K for the spin label TEMPOL (**VI**) are plotted for different temperatures: circles at $T = 19$°C and squares at $T = -6$°C. The solid line is the SE equation (Eq. [4]), which passes through the two points at 0% glycerol. The dashed lines are from Evans' model (Eqs. [6]–[8]). The optimum fit of the model to the data was obtained with $p_1 = 0.71 \pm 0.03$ and $\tau_o = 33.0 \pm 2$ ps at 20°C. Experimental uncertainties are 10% and are on the order of the size of the icons. (B) Normalized rotational correlation times, τ_θ/τ_o, versus η/T, in units of cP/°K for the spin label **I** are plotted for different temperatures: open circles at $T = 60$°C, squares at $T = 33$°C, and triangles at $T = 19$°C; and in different percentage glycerol solutions (0, 30, 70, and 90%, going from left to right) for each fixed temperature. The Evans model gave $p_1 = 0.85 \pm 0.04$ and τ_o 26.5 = 1 ps at 20°C, in water, with a standard error of 0.14. The experimental uncertainties are shown as error bars: ±7% for the 60°C data, and ±4% for the 33 and 19°C data.

of the percentage of glycerol, and fitted the log–log plot to a viscosity power law then we would have found a power law dependence of τ_θ/τ_o on η to the 0.88 $\pm$ 0.02 power with a standard error of 0.18. However this fit is not physically meaningful because it requires the pure water data, taken at different temperatures, to lie at a single point and not on a horizontal line. In contrast Eq. [6] produces a line for each temperature, with the power law dependence of $p_1 = 0.85 \pm 0.04$, with a standard error of 0.10. The overall fit of the Evans model to the data is 70% better than a simple straight line fit, despite both models having two adjustable parameters. Such an improvement with no additional adjustable parameters of the 33 data points is highly significant—more than 3 times the significance criterion of an F test at the 99% confidence level. Inspection of Fig. 3B shows that the model could agree better with the data if the power law exponent were made to depend on temperature; the power would decrease with increasing temperature.

Change of hyperfine splitting (hfs) with concentration. Concentration changes have a noticeable effect on the apparent hfs of the ^{14}N and ^{15}N lines. Figure 4A shows that the hyperfine separations as a function of spin label concentration, [NO], for both spin species, $\bar{a}_j$([NO]) (where j is ^{14}N or ^{15}N) have the same *linear* dependence on concentration (viz., -25 mG/mM). The plots in Fig. 4B show that the hyperfine splittings due to the proton or deuteron are also linearly dependent upon the concentration of spin label, but the dependence is weaker than for the nuclei shown in Fig. 4A. Such a linear dependence of $\bar{a}_j$([NO]) was first reported by Halpern (*14*) for the single axial proton in monoprotonated *d*CTPO (**IV**) where $\bar{a}_H(0) = 0.5$ G. The results presented here show that a linear dependence of $\bar{a}_j$([NO]) with spin label concentration is quite universal for all the magnetic nuclei in spin labels.

What is unusual about this result is that it is completely at odds with the predictions of simple exchange theory for a two-site jump model. The classical text on exchange by Molin (*13*) discusses the way in which exchange broadened lines distort and move as exchange increases. For slow exchange the condition is

$$K_{ex} \cdot [\text{label}] \ll \bar{a}_j, \qquad [14]$$

where K_{ex} is the exchange rate, [label] the label concentration, and $\bar{a}_j$ the hyperfine splitting, which is a function of label concentration. The product $K_{ex} \cdot$ [label] is the two-site hopping rate. Simple two-site jumping theory shows that in slow exchange the lines broaden by an amount $\Delta\omega_{1/2}$:

$$\Delta\omega_{1/2} = K_{ex} \cdot [\text{label}], \qquad [15]$$

and in slow exchange the inward line shift $\delta\omega$ is given by

$$\delta\omega = (K_{ex} \cdot [\text{label}])^2/\bar{a}_j(0), \qquad [16]$$

where $\bar{a}_j(0)$ is the hyperfine splitting at zero spin label concentration. More rigorously,

$$\delta\omega\left(1 + \frac{\delta\omega}{\bar{a}_j(0)}\right) = (K_{ex} \cdot [\text{label}])^2/\bar{a}_j(0), \qquad [17]$$

which should be quadratic in label concentration and inversely proportional to $\bar{a}_j(0)$ in the slow exchange limit (Eqs. [3.2] to [3.4] on page 108 of (*13*)). For ^{15}N spin labels at 1 mM concentration in water, the slow exchange regime applies because of Eq. [14]: $\bar{a}_{^{15}N}(0)$ at 22 G is 100 times greater than $K_{ex} \cdot$ [label], which is approximately 0.2 G (ignoring statistical factor effects) and in excellent agreement with Molin's data in Table 4.22 (*13*). The line broadening predicted by Eq. [15] agrees with the experiment as already discussed.

How do the experimentally determined line shifts compare with theory? Figure 5 plots the dependence of the slope of the hyperfine splitting with label concentration, $-\partial(\bar{a}_j)/\partial$[NO], vs the magnitude of $\bar{a}_j(0)$. The experimental data could not be more at odds with the predictions of Eqs. [16] or [17]: For example, for 1 mM ^{15}N label in solution the theoretical $\delta\omega$ is about 9 mG whereas the experimental value is at 25 mG. (Fortuitously, the experiment and theory agree when the label concentration is around 2.5 mM.) All attempts to fit the data to the quadratic form of Eq. [16] failed. The observed shift is *linear* (not quadratic) in concentration and is *not* inversely proportional to $\bar{a}_j$, which is a sensitive test of the validity of Eq. [16]. At the smaller hyperfine splitting of 190 mG (arising from methyl protons) and 30 mG (methyl deuterons)—where $K_{ex} \cdot [\text{label}] > \bar{a}_j$ and one is no longer in slow exchange—the concentration effect is *still* linear. The shifts with concentration are linear and independent of $\bar{a}_j(0)$ over a 40-fold range of hyperfine splitting (from $\bar{a}_j = 22$ G for ^{15}N to $\bar{a}_j = 0.5$ G for an axial proton). *Never* does $\delta\omega$ increase as $\bar{a}_j$ becomes smaller.

Halpern has suggested Eq. [2.142] on page 68 of the Molin text (*13*) to explain the result. This equation is

$$\delta\omega = -\delta_j \cdot \tau \cdot K_{ex} \cdot [\text{label}]/2. \qquad [18]$$

Usually $\delta_j = 2\bar{a}_j$ and τ is the contact time for the collision, which is on the order of the rotational correlation time (*21*). Equation [18] can be modified to agree with the experimentally observed data over the entire hfs range if we make $\tau = 1/R_{1e}$ and redefine δ_j to be $2/\delta_j = 1/\bar{a}_j + 1/R_{2e}$ so that

$$\frac{\delta\omega}{[\text{label}]} = -K_{ex} \cdot \bar{a}_j(0) \cdot \frac{R_{2e}/R_{1e}}{\bar{a}_j(0) + R_{2e}}, \qquad [19]$$

where $R_{1e} \sim 1$ G and $R_{2e} = 0.13$ G. In the limit where $\bar{a}_j$ is small Eq. [19] goes to Eq. [18] and when $\bar{a}_j$ is large $\delta\omega$ becomes independent of $\bar{a}_j$ as required for agreement with the experiment as shown in Fig. 5. Equation [19] points up the

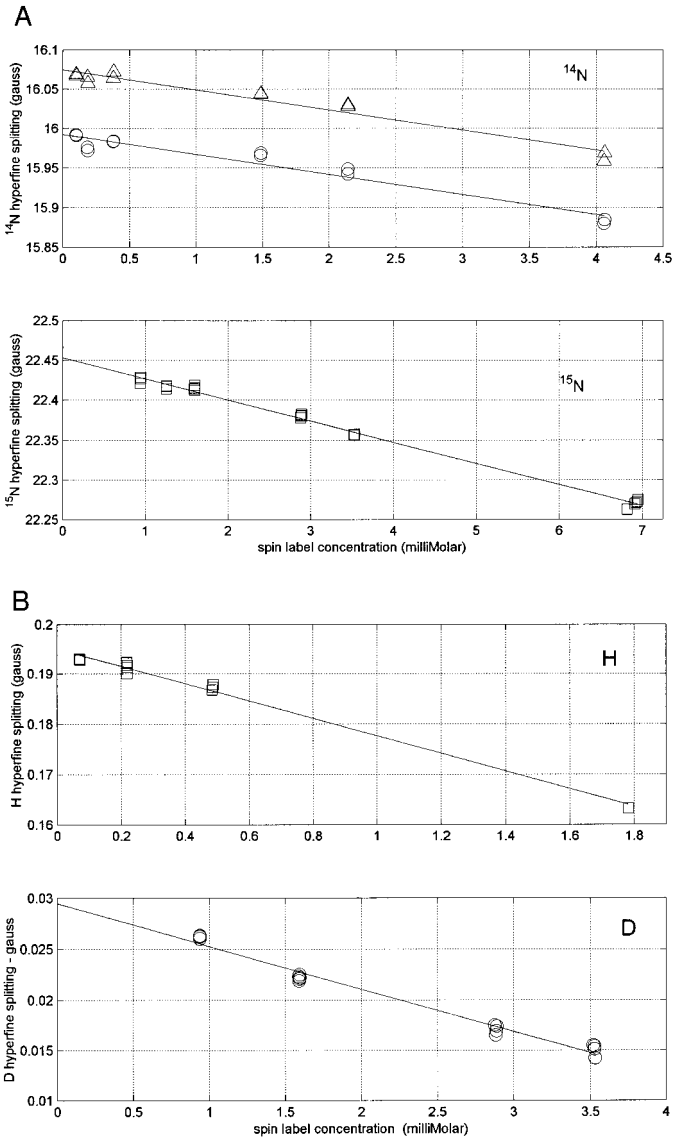

FIG. 4. (A) Plots of the hyperfine separations, $\bar{a}$, as a function of the spin label concentration [NO], $\bar{a}_j$([NO]) for species j, where $j = {}^{14}$N (top) or $j = {}^{15}$N (bottom). The hyperfine separations of the ^{14}N and ^{15}N lines have a linear dependence on concentration of spin label. (Top) The field separation of the high-field line ($m = -1$) from the center line ($m = 0$) versus concentration is shown as triangles for (**III**). The best straight line fit shown as a solid line gave an intercept of 16.074 ± 0.003 G with a slope of −0.025 ± 0.002 G/mM spin label. For the difference between the center line ($m = 0$) and the low-field line ($m = +1$) versus concentration the data (circles) were fit to the solid straight line with an intercept of 15.992 ± 0.004 G with a slope of −0.025 ± 0.002 G/mM. The intercepts are not the same because the three EPR lines are unequally spaced due to second order effects (*23*). The standard error of the upper and lower fits are 0.009 and 0.008 G, respectively. (Bottom) For the ^{15}N label (**I**), the field separations of the high-field line ($m = -\frac{1}{2}$) from the lower line ($m = +\frac{1}{2}$) vs concentration are shown as circles. The best straight line fit (shown as a solid line) had an intercept of 22.450 ± 0.002 G with a slope of −0.0265 ± 0.0004 G/mM spin label. The standard error of the fit was 0.004 G. The experimental uncertainties are the size of the data points in all plots. (B) The linear dependence on concentration of spin label for the splittings of the 12 methyl protons (H) in (**III**) (top) and the corresponding 12 methyl deuterons (*D*) in (**I**) (bottom). (Top) The data are shown as squares and the solid line is the best fit with a zero label concentration intercept of 0.195 ± 0.0003 G with a slope of −0.0174 ± 0.0006 G/mM. The standard error of the fit was 0.001 G. (Bottom) The data are shown as circles and the solid line is the best fit with an intercept of 0.0295 ± 0.0004 G and with a slope of −0.0042 ± 0.0002 G/mM. The standard error of the fit was 0.0006 G. The experimental uncertainties are the size of the data points in all plots.

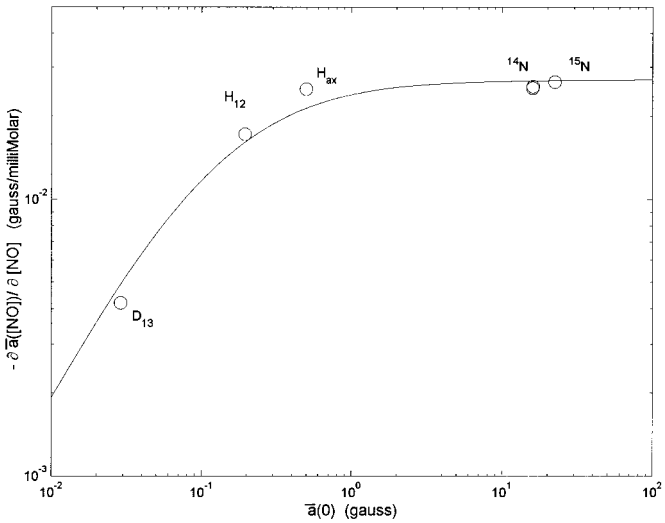

FIG. 5. Plot of the dependence of the slope of the hyperfine splitting with label concentration, $-\partial(\bar{a})/\partial$[NO], vs the magnitude of $\bar{a}(0)$. The empirical formula to fit these data is Eq. [19]: $\delta\omega/[\text{label}] = (0.027 \cdot \bar{a}_j)/(\bar{a}_j(0) + 0.13)$ with $K_{ex} \cdot R_{2e}/R_{1e} = 0.027$ and $R_{2e} = 0.13$ G. The experimental uncertainties (obtained from Fig. 4) are the size of the data points.

dependence of the shift on the relative magnitudes of $\bar{a}_j$ and R_{2e}. The apparent dependence upon some slow process, such as the suggested R_{1e} process, might appear surprising and is not consistent with the original derivation of Eq. [18] in the Molin text (*13*). Such a purely empirical explanation underscores the discrepancy between theory and experiment and hopefully points the way to how the theory needs to be modified.

We emphasize that the experimental linewidth *broadening* with concentration *does* fit Molin's theoretical model of Eq. [15], even though the quadratic line shift predicted by Eq. [16] does not. We were concerned that our data analysis methodology was the source of the problem. In the companion paper (I) we noted the failure of the program to fit the data at high concentrations (>2–3 mM). We therefore simulated two-site jump spectra based on the Molin model and analyzed the simulated lineshapes with our data analysis program. The results showed that the linewidth did increase in agreement with Eq. [15] and the line shift did change quadratically according to Eq. [16]. Therefore, we can rule out the possibility that the analysis program somehow produced a linear shift in an attempt to fit the spectra, missing the subtleties of the two-site jump lineshapes. We speculate that the answer to the disagreement must, at the very least, involve a reinterpretation

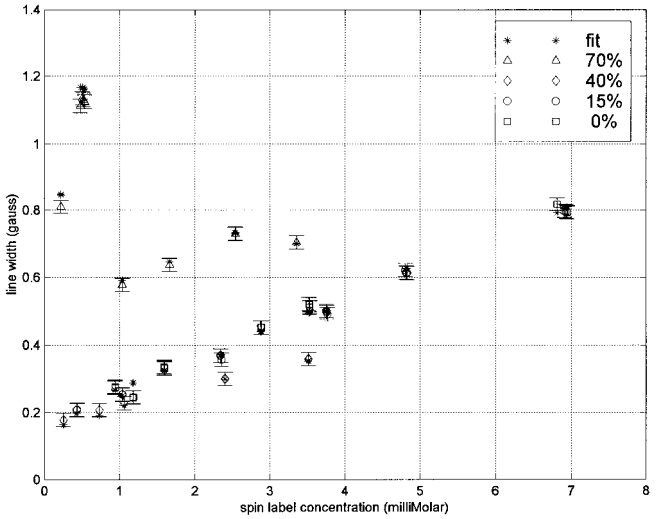

FIG. 6. A plot of calculated linewidths, $\bar{R}_{2e}^{calc}$, (*) compared to $\bar{R}_{2e}$, the mean homogeneous linewidths of the two lines of $^{15}ND_{13}$ *d*CTPO (**I**) in 0% (squares), 15% (circles), 40% (diamonds), and 70% (triangles) glycerol over the range of spin label concentrations shown on the *x* axis. The O_2 concentrations ranged from 0.095 to 0.28 mM and arose from the different solubility of O_2 in various percentages of glycerol and with temperature. The temperature for these 72 experimental data points varied only from 17 to 22°C. The model used for the fit is Eq. [13]. The optimum values were $a_1 = 0.45 \pm 0.04$ (for the spin label) and $b_1 = 0.42 \pm 0.2$ (for oxygen). The relaxivities were 92 ± 2 and 420 ± 20 mG/mM for spin label and O_2, respectively. The standard error of the theoretical fit to the data was 0.018 G. The inherent reproducibility of experimental results gave an uncertainty of ± 0.010 G and is shown as error bars.

of the contact time. It is more likely the answer lies with a different dynamic model for the nitroxide–nitroxide interactions which takes into account the nature of the translational motion and the collisions between labels.

The experimental linewidths $\bar{R}_{2e}$ (computed as the average of the two linewidths in the ^{15}N spectrum) of spin label (**I**) in 0, 15, 40, and 70% glycerol are plotted as a function of spin label concentration in Fig. 6. The $\bar{R}_{2eo}$ term is a known quantity for each datum point being computed from τ_θ as calculated from the experimental *B* parameter using the Goldman equations (*1*). The percentages of glycerol, as well as the concentrations of nitroxide and oxygen, are all known. The only adjustable constants are C'_{NO} and C'_{O_2} (the relaxivities in water at $T_o = 20$°C) and a_1 and b_1. We can therefore fit the data to the model described by Eq. [13] to obtain the linewidths, $\bar{R}_{2e}^{calc}$, which are also shown in the figure. The optimum values of $p_{NO} = a_1 = 0.45 \pm 0.04$ (for the spin label) and $p_{O_2} = b_1 = 0.42 \pm 0.2$ (for oxygen) are the power law dependencies for the nitroxide and for oxygen collision processes in 100% glycerol. The power dependence of oxygen reported here is in good agreement with values of $p_{O_2} = 0.53 \pm 0.08$ based on the kinetics of diffusion-controlled transport of oxygen to myoglobin in water/glycerol mixtures (*22*) and of $p_{O_2} = 0.48 \pm 0.05$ from the measurements of Jordan *et al.* (*10*). The relaxivities in water at 20°C for the spin labels and O_2 are 92 ± 2 and 417 ± 20 mG/mM, respectively. Hence, by adjusting the power law dependencies to be approximately 0.5 for both the spin label and the oxygen, we find excellent agreement between the predictions of theory and the experimental data. No adjustable extra term need be added to the homogenous linewidths extracted from the CW experiments. The extent of the agreement is within the experimental uncertainties. The rather large uncertainty in the power for the O_2 arises because oxygen broadening rapidly decreases as the glycerol percentage rises. This is due to reduced translational diffusion and to reduced oxygen solubility.

CONCLUSIONS

The most important conclusion of this work is that the experimental linewidths of spin labels in liquids can be completely explained. The combination of the END and SR theory applied to linewidths plus exchange interactions can quantitatively predict the experimental linewidths of the lines. The relaxivities of model nitroxides over a range of viscosities is now calibrated. A straightforward prescription for interpreting linewidths in terms of rotational motion is now established. The power law dependencies of the rotational correlation times on viscosity go as the 0.7 to 0.8 power of the viscosity in higher percentage glycerol mixtures. The power law dependencies of the translational diffusion coefficients on the viscosity are of order 0.5. Neither process for glycerol therefore obeys the SE relation, although the rotational motion is clearly closer to it. The simple SE prediction that translational correlation time is simply proportional to the rotational correlation times is not observed because of the ~0.7 power dependence found. This power law dependence is very much consistent with the previous experiments by Evans.

We now have a calibrated method to measure rotational correlation times. Different models for motion can be easily tested as both absolute linewidths *and* the relative differences in linewidths must be explained by the same model.

Very subtle effects on the lines can be measured—second order splitting and shifts due to changes in concentration. This latter effect should be useful as a method of concentration measurement, as pointed out by Halpern. We have demonstrated it to be applicable to *any* hfs splitting in any spin label and remove the requirement of any special isotopic substitution.

Table 1 shows that the SF of the nitrogen nuclei have the major effect on the broadening, with the axial protons on the label ring having a lesser effect. The measurement of oxygen concentration also now does not require special labels, as the linewidth analysis is sensitive enough to observe the very small changes due to the oxygen—tens of milligauss—even when the natural linewidths are hundreds of milligauss. The relative magnitudes of the relaxivities of oxygen and the spin labels have been explained, leading to the conclusion that the translational diffusion processes for oxygen and spin labels in

viscous media appear similar. Our results show that oxygen relaxes ^{14}N labels slightly more strongly than ^{15}N labels.

ACKNOWLEDGMENTS

We thank NIH for support for this work on P01-GM32681 and for a training grant for A. W. Reese. The EMX EPR spectrometer used was funded under the UW Environmental Sciences Center Grant P30-ESO7033 from NIEHS. Thanks are due to Dr. M. K. Bowman for helpful insight into translational diffusion processes and to Dr. Howard Halpern for a gift of the monoprotonated ^{15}N *d*CTPO spin label.

REFERENCES

1. J. S. Hwang, R. P. Mason, L. P. Hwang, and J. H. Freed, *J. Phys. Chem.* **79,** 489–511 (1975).
2. A. G. Redfield, *Phys. Rev.* **98,** 1787–1800 (1955).
3. B. H. Robinson, C. Mailer, and A. W. Reese, *J. Magn. Reson.* **138,** 199–209 (1999).
4. B. H. Robinson, A. W. Reese, and C. Mailer, 37th Rocky Mountain Conference on Analytical Chemistry, Denver, CO (1995).
5. W. K. Subczynski and J. S. Hyde, *Biophys. J.* **45,** 743–748 (1984).
6. R. E. D. McClung and D. Kivelson, *J. Chem. Phys.* **49,** 3380–3391 (1968).
7. M. J. Povich, *J. Phys. Chem.* **79,** 1106–1109 (1975).
8. D. A. Haas, T. Sugano, C. Mailer, and B. H. Robinson, *J. Phys. Chem.* **97,** 2914–2921 (1993).
9. D. F. Evans, T. Tominaga, and H. T. Davis, *J. Chem. Phys.* **74,** 1298–1305 (1981).
10. J. Jordan, E. Ackerman, and R. L. Berger, *J. Chem. Phys.* **78,** 2979–2983 (1956).
11. W. K. Subczynski and J. S. Hyde, *Biophys. J.* **41,** 283–286 (1983).
12. K. M. Salikhov, A. B. Doctorov, Y. N. Molin, and K. I. Zamaraev, *J. Magn. Reson.* **5,** 189–205 (1971).
13. Y. N. Molin, K. M. Salikhov, and K. I. Zamaraev, "Spin Exchange: Principles and Applications in Chemistry and Biology," Springer-Verlag, Berlin (1980).
14. H. J. Halpern, M. Perc, T.-D. Nguyen, B. A. Teicher, Y. J. Lin, and M. K. Bowman, *J. Magn. Reson.* **90,** 40–51 (1990).
15. T. I. Smirnova, A. I. Smirnov, R. B. Clarkson, and B. L. Belford, *Magn. Reson. Med.* **33,** 801–810 (1995).
16. C. Mailer, D. A. Haas, E. J. Hustedt, J. G. Gladden, and B. H. Robinson, *J. Magn. Reson.* **91,** 475–496 (1991).
17. Zeus, Inc., Orangeburg, SC.
18. A. I. Smirnov, S.-W. Norby, J. A. Weyhenmeyer, and R. B. Clarkson, *Biochim. Biophys. Acta* **1200,** 205–214 (1994).
19. J. S. Hyde and W. K. Subczynski, *in* "Spin Labeling: Theory and Applications" (L. J. Berliner and J. Reuben, eds.), Vol. 8, p. 399–425, Plenum, New York (1989).
20. A. Abragam, "The Principles of Nuclear Magnetism," Oxford Univ. Press, Oxford (1961).
21. D. Kivelson, *J. Chem. Phys.* **33,** 1094–1106 (1960).
22. B. B. Hasinoff and S. B. Chishti, *Biochemistry* **22,** 58–61 (1983).
23. J. E. Wertz and J. R. Bolton, "Electron Spin Resonance Elementary Theory and Practical Applications," McGraw–Hill, New York (1972).
24. J. S. Hyde and W. K. Subczynski, *J. Magn. Reson.* **56,** 125–130 (1984).
25. M. K. Bowman, T. J. Michalski, M. Peric, and H. J. Halpern, *Pure Appl. Chem.* **62,** 271–274 (1990).
26. H. J. Halpern, M. Peric, C. Yu, and B. L. Bales, *J. Magn. Reson. A* **103,** 13–22 (1993).
27. A. I. Smirnov and R. L. Belford, *J. Magn. Reson. A* **113,** 65–73 (1995).
28. P. D. I. Morse and A. I. Smirnov, *Magn. Reson. Chem.* **33,** S46–S52 (1995).
29. R. Battino, H. L. Clever, and C. L. Young, "The Solubility of Gases in Liquids," Pergamon, Elmsford, NY (1981).